Journal of Crystal Growth 81 (1987) 304–313
North-Holland, Amsterdam

DELTA- (δ-) DOPING IN MBE-GROWN GaAs: CONCEPT AND DEVICE APPLICATION

Klaus PLOOG

Max-Planck-Institut für Festkörperforschung, D-7000 Stuttgart-80, Fed. Rep. of Germany

The implementation of δ-function-like doping profiles during molecular beam epitaxy (MBE) of GaAs by using Si donors and Be acceptors is employed to generate V-shaped potential wells with a quasi-two-dimensional electron (hole) gas and to create a new GaAs sawtooth doping superlattice with strongly reduced energy gap. Three examples for application of δ-doped n-type GaAs are given; (i) as electron supplying layer in selectively doped asymmetric GaAs/$Al_xGa_{1-x}As$ quantum well heterostructures, (ii) as thin tunneling barrier for non-alloyed ohmic contacts on n-GaAs, and (iii) as Schottky gate δ-doped field effect transistor. GaAs sawtooth doping superlattices are attractive for application in photonic devices due to the significant red-shift of their luminescence.

1. Introduction

The term delta- (δ)- doping stands, strictly speaking, for the confinement of dopant atoms during crystal growth to a two-dimensional (2D) plane one atomic layer thick. This doping concept, also called atomic-plane or sheet doping, during molecular beam epitaxy (MBE) of GaAs was originally proposed to improve the doping profile of Ge-doped n-type GaAs layers [1]. With the increasing importance of 2D carrier systems in semiconductors for device application and for fundamental studies, the implementation of δ-function like doping profiles by using Si donors and Be acceptors has been employed to generate symmetric, V-shaped potential wells in GaAs with a quasi-2D electron (hole) gas [2], and to create a new GaAs sawtooth doping superlattice (SDS) with a strongly reduced effective energy gap [3].

In this concise review we first discuss the concept of δ-doping in GaAs and the existence of quantized energy levels in the V-shaped potential well. A brief account on sample preparation by MBE follows in section 3. Then three areas for application of δ-doped n-type GaAs are given in section 4; (i) as electron supplying layer in selectively doped (SD) asymmetric GaAs/$Al_xGa_{1-x}As$ quantum well heterostructures (QWH) to reduce the undesired persistent photoconductivity (PPC) effect in high-electron mobility transistors (HEMTs) operating at 77 K, (ii) as thin tunnelling barrier for non-alloyed ohmic contacts on n-GaAs having a low specific contact resistance, and (iii) as Schottky gate δ-doped field effect transistor (δ-FET) with high transconductance due to the narrow spacing between the electron channel confined to the atomic impurity plane and the gate metal. Finally, in section 4.4 we discuss periodic δ-doping layer structures and in particular the properties of GaAs sawtooth doping superlattices which are promising for application in photonic devices due to the significant red-shift of their luminescence also at room temperature.

2. Concept of δ-doping

The basic concept of δ-doping in GaAs is illustrated in fig. 1. The Si donors are located in an atomic monolayer of the (100) oriented GaAs host material, and the ionized donors provide a continuous positive sheet of charge. The fractional coverage of the available Ga sites in the (100) plane can reach several percent. The impurity charge distribution N_D can mathematically be described by the Dirac delta function, i.e. $N_D = N_D^{2D}\delta(z)$, where N_D^{2D} is the 2D donor concentration. Due to electrostatic attraction the electrons remain close to their parent ionized donors and form a quasi-2D electron gas (2DEG) in the V-shaped potential well produced by the positive sheet of charge. In the narrow potential well the

0022-0248/87/$03.50

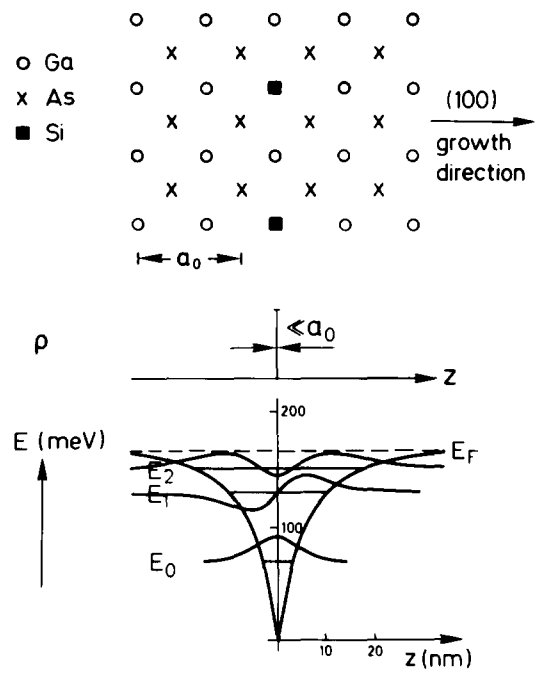

Fig. 1. Schematic illustration of δ-doping in GaAs. The Si donors are located in an atomic monolayer of the (100) GaAs host crystal (top). A V-shaped potential well is formed (bottom). The subband energies and wavefunctions are calculated selfconsistently assuming a uniform sheet of positive charge.

electron energies for motion perpendicular to the (100) growth surface are quantized into 2D subbands. The subband levels have been calculated by a simple approximation [4], taking into account band bending of the conduction band due to localized ionized impurities and to free carriers, and in a more elaborate way also selfconsistently taking into account the non-parabolicity of the conduction band [2]. Direct evidence for the formation of 2D subbands in δ-doped GaAs came from Shubnikov–De Haas (SdH) oscillations observed during magnetotransport measurements with the magnetic field perpendicular to the sample [2].

Two phenomena make the concept of δ-doping different from other 2D carrier systems. First, even at moderate δ-doping concentrations the electrons populate already several excited subbands. At a doping concentration of 4×10^{12} cm^{-2} four subbands and at 1×10^{13} cm^{-2} seven subbands are occupied [4]. In contrast to the 2DEG of SD heterostructures, electrons in δ-doped samples populating the ground-state subband exhibit the lowest mobility in comparison to the excited subbands, due to the proximity of the bare ionized impurities. This decrease in electron mobility with decreasing subband index was clearly observed in the magnetotransport measurements [2]. The second difference is the considerable delocalization of the carriers in the dopant plane, i.e. the electronic states are spread out over the ionized donors that form the V-shaped potential well. The real-space extent of the lowest subband reaches 5 to 10 nm for δ-doping concentrations ranging from 1×10^{13} to 1×10^{12} cm^{-2} [4]. Although this means that the characteristic binding length of the ground-state electrons is approximately 5 nm, this value is still significantly less than the 20 nm diameter of the hydrogen-like 1s orbit.

3. Sample preparation

The δ-doped GaAs samples were grown by MBE on (100) oriented GaAs substrates using a growth rate of 1 μm/h and a growth temperature $500 < T_s < 550$°C. The δ-function like Si and Be doping profiles were obtained by interrupting the growth of the GaAs host crystal by closing the Ga shutter and leaving the As shutter open. The As-stabilized surface reconstruction was thus maintained, while the shutter of the respective dopant effusion cell was opened for a certain time interval (up to several minutes for high δ-doping levels). In this impurity growth mode the host crystal does not grow. To continue GaAs growth, the dopant shutter was closed and the Ga shutter was opened again. For single-type δ-doping layers in GaAs we show in fig. 2 that the measured doping density is in good agreement with the number of supplied dopant atoms up to very high doping densities. The fractional coverage of the available Ga sites in the (100) plane reaches about 5% if we assume that the GaAs (100) surface contains 6.25×10^{14} Ga atoms cm^{-2}. At these high doping levels the surface reconstruction displayed in the RHEED pattern changes from the As-stabilized (2 × 4) to a (1 × 3) reconstruction. When low growth tempera-

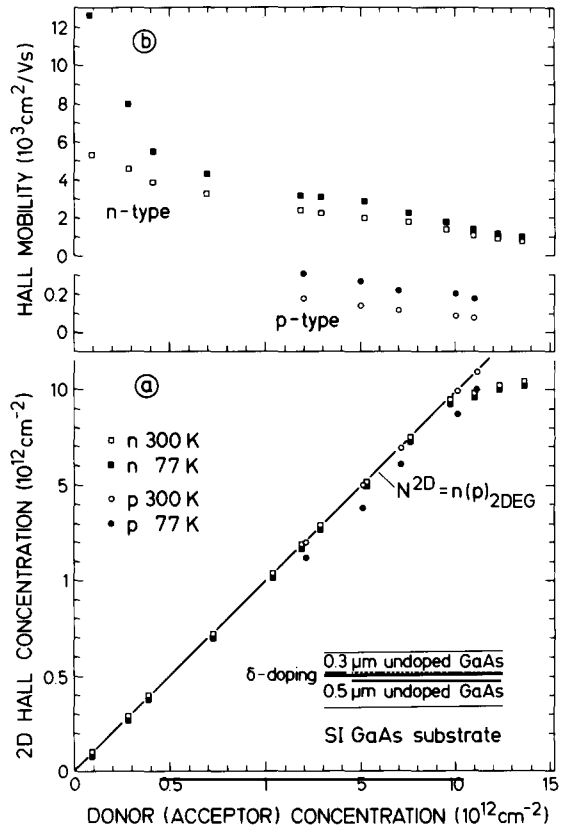

Fig. 2. 2D Hall concentration versus supplied dopant atoms in single n- and p-type δ-doped GaAs (a) and Hall mobility versus supplied dopant atoms measured at 300 and 77 K (b).

tures are employed, which is particularly important for Be-δ-doping , the surface morphology of the epilayers remains atomically smooth also at high doping densities.

In Be-δ-doped GaAs, hole densities as high as 2×10^{13} cm^{-2} were easily achieved without any indication of saturation. A certain carrier freeze-out was observed in samples cooled to 77 K (no further freeze-out occurs down to 4 K). This phenomenon is not yet fully understood. In Si-δ-doped GaAs, we observed a deviation of measured electron density from the supplied dopant atoms beyond 1×10^{13} cm^{-2}. At these high doping densities the electrons in the V-shaped potential well populate high-index subbands so that the Fermi energy is increased by more than 300 meV [4]. This energy shift is comparable with the energy separation between Γ and L conduction band minima in GaAs. Electrons may thus populate the L minimum at high Si doping levels. No carrier freeze-out occurs for Si-δ-doping, in agreement with homogeneous doping, also not in the saturation regime. The Hall mobilities measured for both n- and p-type δ-doping compare favourably with homogeneous doping (fig. 2b).

In fig. 3 we show the measured capacitance–voltage (C–V) profile of a δ-doped GaAs layer grown on n$^+$-GaAs substrate with the 2DEG located 70 nm below the rectifying metal–semiconductor contact. The narrow full-width at half-maximum of 4.6 nm, which does not change with reduced temperature, manifests the confinement of the Si donors to an atomic plane. The independence on temperature implies, however, that we cannot interpret the C–V profiles obtained from δ-doped GaAs by means of the conventional Debye–Hückel screening length limitations. Therefore, we have recently developed a model for the C–V profiles of δ-doping taking into account the quantum-size effect [5]. This interpretation clearly shows that the measured profiles reflect neither the dopant nor the free-carrier concentration profile. Instead, they reflect the shift of the electron wavefunction in the V-shaped potential well, which is tilted by the applied voltage. In this way a good agreement between measured and calculated C–V profiles can be obtained.

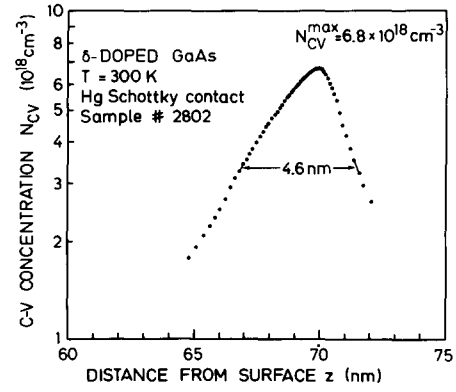

Fig. 3. C–V profile of a δ-doped GaAs sample measured at room temperature. The peak of the profile is located at the depth of the δ-doping layer beneath the surface derived from the growth parameters.

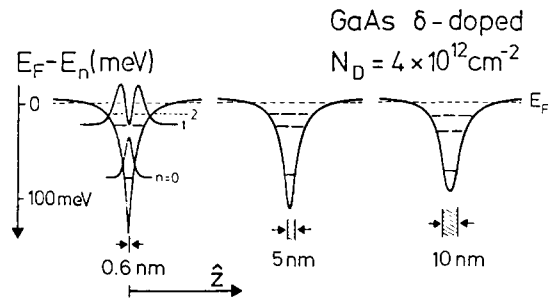

Fig. 4. Variation of potential well and subband levels in δ-doped GaAs as a function of broadening of the doping profile. The selfconsistent calculations were performed for a δ-doping concentration of 4×10^{12} cm^{-2} in a p-type background doping. The energies of the three occupied levels on the left-hand side are 78, 26, and 10 meV respectively, below the Fermi energy E_F.

The C–V profile shown in fig. 3 is narrower than the spatial extent of the lowest subband and thus indicates a confinement of the Si dopant atoms to an atomic layer in the GaAs host material. The influence of a smearing of the Si doping beyond the (100) atomic plane on the subband levels has been calculated recently [6]. Fig. 4 shows schematically that the depth of the potential well is very sensitive, while the subband energies (and the population) vary only slowly with a spreading of the donor ions. Since the experimental determination of subband energies has error limits of typically 5 to 10%, a smearing of 5 nm cannot be detected reliably. However, a 10 nm broadening of the doping profile is easily identified by examination of the $n=0$ and $n=1$ energy separation. We have experimentally confirmed that a sample with two δ-doped layers of 2×10^{12} cm^{-2} each separated by 3 nm undoped GaAs exhibits the same magnetotransport properties as a GaAs sample with just one δ-doped layer of 4×10^{12} cm^{-2}.

4. Results and discussion

4.1. High-mobility 2DEG from δ-doped asymmetric quantum wells

Due to the close proximity of ionized impurities and free carriers, the Hall mobility of 2D carriers measured in δ-doped GaAs is comparable to homogeneously doped material of the same doping concentration. We have recently developed a new semiconductor structure having the 2DEG spatially separated from the δ-doped ionized impurities [7]. The characteristic feature of the new 2DEG (or 2D hole gas: 2DHG) structure is a narrow asymmetric quantum well which is δ-doped at its centre. A spatial separation of only 10 nm is sufficient to produce a mobility enhancement as high as 10^6 cm^2/V · s at 5 K.

In fig. 5a we show that in two types of an asymmetric GaAs quantum well no quantized states are formed if the well width L_z is smaller than a critical value. The maximum well width before a bound state is formed in the asymmetric well is $L_z \cong 2.5$ nm when we choose the alloy compositions $Al_{0.4}Ga_{0.6}As$ and $Al_{0.1}Ga_{0.9}As$ for the asymmetric barriers. If such a narrow asymmetric well is doped, the electrons (or holes) from the respective donors (or acceptors) are *not* confined in the well. They are instead transferred and form a 2DEG (or 2DHG) at the adjacent heterojunction (fig. 5b). The ternary $Al_xGa_{1-x}As$ barriers of this structure remain undoped, and so the undesired persistent photoconductivity effect due to deep donors in n-type $Al_xGa_{1-x}As$: Si is less pronounced. In addition, the high-mobility 2DEG can be located close to the crystal surface. A narrow spacing between the 2DEG and the gate

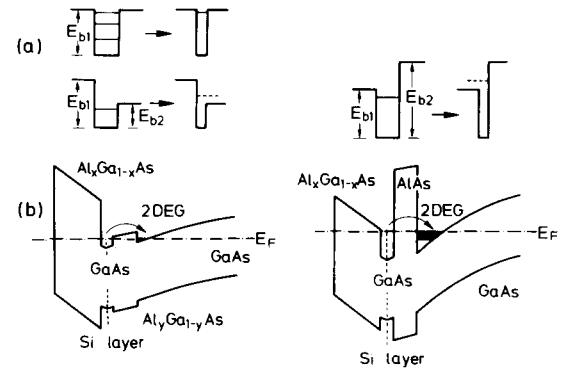

Fig. 5. Schematic illustration of (a) formation of bound electron states in symmetric and asymmetric quantum wells and (b) formation of high-mobility 2DEG from δ-doped asymmetric $Al_xGa_{1-x}As/GaAs/Al_yGa_{1-y}As$ (left) and $Al_xGa_{1-x}As/GaAs/AlAs$ (right) quantum well heterostructure.

metal is important for high transconductances in FETs fabricated from these heterostructures.

The temperature dependence of the Hall mobility obtained from several δ-doped asymmetric QWH of different configuration are displayed in figs. 6 and 7. The spatial separation of the 2DEG from the monolayer of ionized Si donors leads to a mobility enhancement by a factor of three even at room temperature. The difference between the Si-δ-doping density (2×10^{12} cm^{-2}) and the measured 2DEG density is used to establish the surface potential of the $Al_{0.4}Ga_{0.6}As$ layer covered by a 1 nm GaAs cap layer. With reduced sample temperature a strong mobility enhancement is observed. The highest mobilities are achieved for δ-doped asymmetric QWH with AlAs spacer where the electrons of the 2DEG have to tunnel through a 10 nm barrier. The measured peak mobility of 10^6 cm^2/V·s is the highest ever reported for a SD

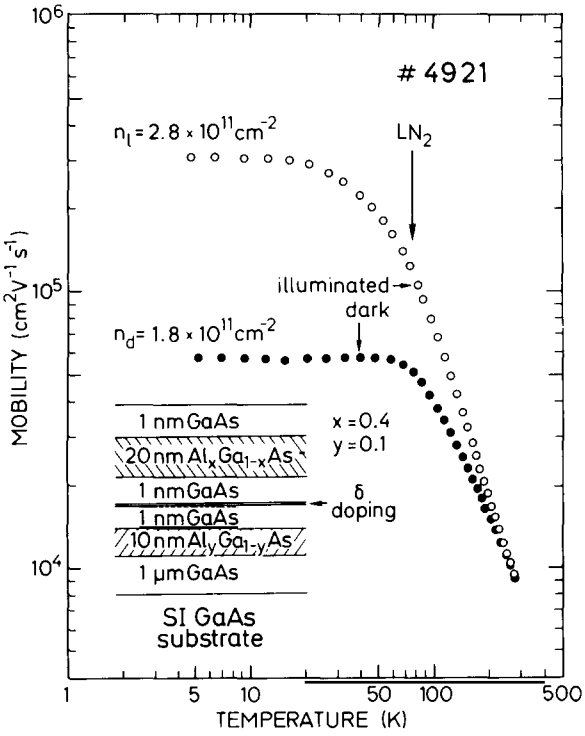

Fig. 6. Hall electron mobilities versus temperature obtained from the δ-doped asymmetric $Al_{0.4}Ga_{0.6}As$/GaAs/$Al_{0.1}Ga_{0.9}As$ quantum well heterostructure whose configuration is shown schematically in the inset.

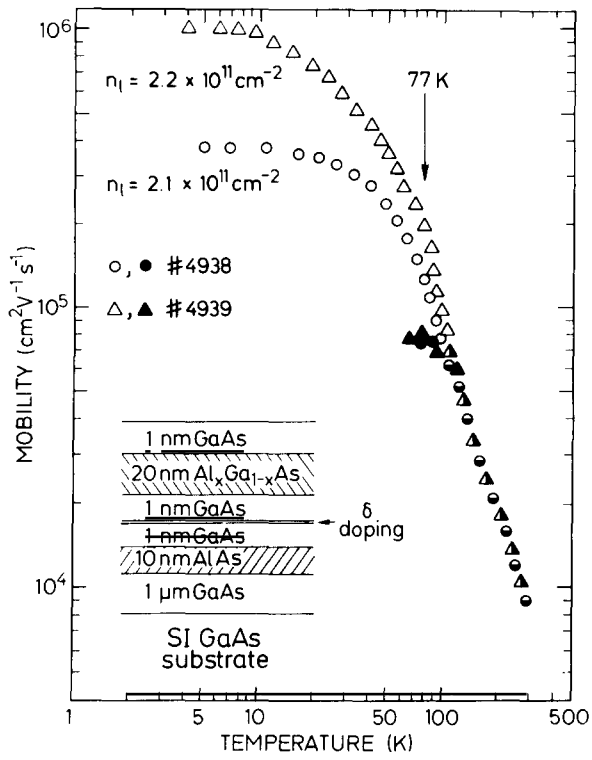

Fig. 7. Hall electron mobilities versus temperature obtained from two δ-doped asymmetric $Al_{0.4}Ga_{0.6}As$/GaAs/AlAs quantum well heterostructures with different δ-doping densities of $N_D^{2D} = 2 \times 10^{12}$ cm^{-2} and $N_D^{2D} = 3 \times 10^{12}$ cm^{-2}.

GaAs/$Al_xGa_{1-x}As$ heterostructure with a spacer of only 10 nm. It is important to note that the mobility enhancement observed in the new heterostructure at 5 K after illumination is much more pronounced than in conventional SD heterostructures. In addition, the observed increase of the carrier density due to PPC at low temperatures is smaller, and the temperature dependence of the carrier density is totally different. As the concentration of deep donors in the undoped $Al_xGa_{1-x}As$ is low, a substantial contribution to photoconductivity originates from band-to-band electron–hole pair generation in the GaAs buffer layer and subsequent charge separation [8]. The photogenerated electrons are transferred to the 2DEG, while the holes drift toward the semi-insulating substrate where they are trapped by ionized acceptors.

4.2. Non-alloyed ohmic contacts by thin tunneling barriers in δ-doped GaAs

The preparation of low-resistance ohmic contacts is one of the most important steps in the fabrication process of advanced semiconductor devices. We have recently demonstrated tunnelling between the subbands of a δ-doping layer embedded in GaAs 20 nm below the surface and the surface metal [9]. In fig. 8 we show schematically that tunnelling occurs in the selfconsistent potential profile induced by the δ-doping layer and the potential offset at the metal–semiconductor interface. In the derivative of the tunnelling current versus gate voltage measured at 4.2 K, we have observed a distinct fine structure arising from the subband related quantum steps in the density of states of the 2D layer. The deduced subband energies are in good agreement with selfconsistent calculations using the material design parameters of the studied samples.

The scheme of fig. 8 is frequently used to illustrate the formation of ohmic contacts by heavy doping of the semiconductor. For the experiments described above, the contact and depletion region was dimensioned for weak tunnelling to determine the subband energies in the degenerate doping sheet. In order to produce low-resistance ohmic contacts to the semiconductor, we have to reduce the width of the tunnelling barrier significantly so that tunnelling through the barrier dominates the vertical transport properties. We have examined this idea by placing a δ-doping layer with a density of $N_D^{2D} = 1.2 \times 10^{13}$ cm^{-2} just 2.5 nm below the surface. Additional five δ-doping layers separated by 2.5 nm each were placed beneath the contact layer to make the epitaxial layer on the n$^+$-GaAs substrate also n-type. The metal contacts were formed by successively depositing 20 nm Cr and 200 nm Au in a separate vacuum chamber through a Mo shadow mask with holes of 750 μm diameter. The current voltage characteristic displayed in fig. 9 shows strictly linear behaviour on all scales of the curve tracer. We have estimated a specific contact resistance below 10^{-6} Ω cm^2 for these non-alloyed ohmic contacts. In accordance with all studied δ-doped GaAs samples also the δ-doped ohmic contacts have an excellent smooth surface morphology.

4.3. Schottky gate δ-doped field effect transistor (δ-FET)

In the last decade modifications of the doping profile of Schottky gate FETs to improve the device characteristics have been reported by several authors [10,11]. The buried-layer devices, which have the bulk of their doping in a narrow buried layer separated from the gate by a distance large

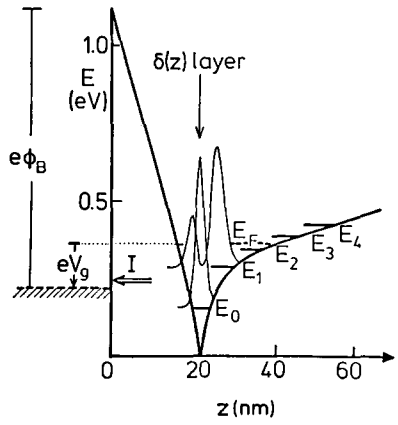

Fig. 8. Schematic illustration of tunneling occuring between the selfconsistent potential profile induced by the δ-doping layer and the potential offset at the metal–semiconductor interface ($N_D^{2D} = 1.4 \times 10^{13}$ cm^{-3}, $\phi_B = 0.90$ V, $V_g = 0.15$ V).

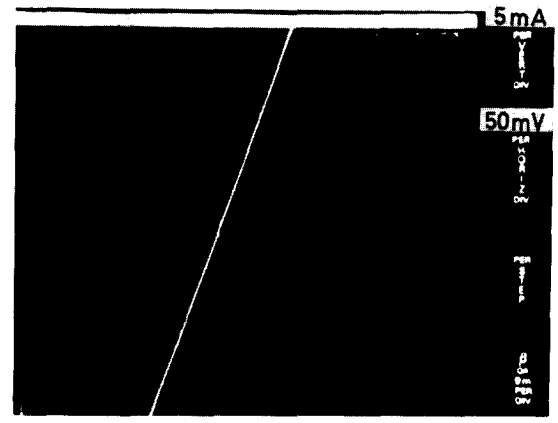

Fig. 9. Current–voltage characteristic of non-alloyed δ-doped ohmic contact to n-GaAs.

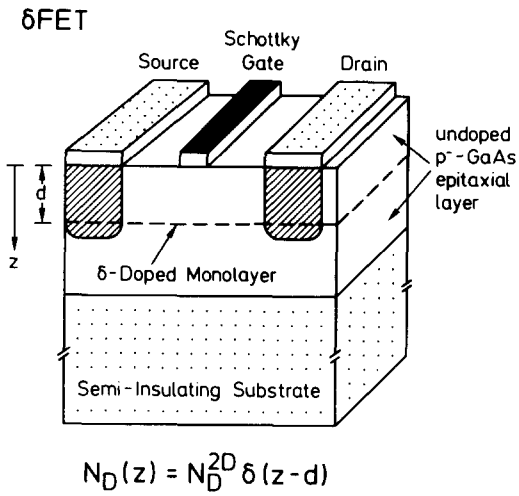

Fig. 10. Schematic illustration of a Schottky gate δ-doped field-effect transistor (δ-FET).

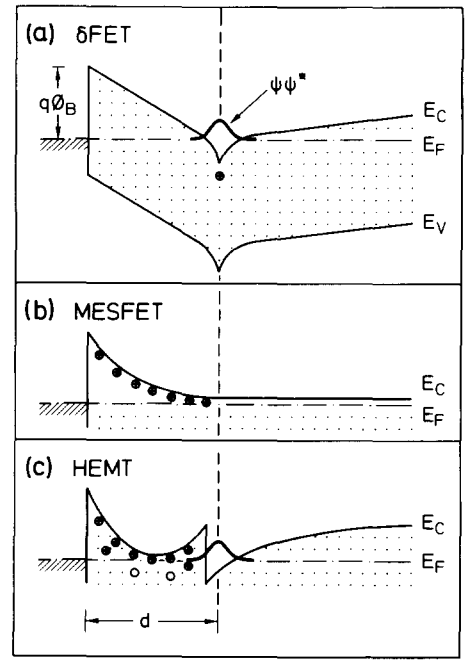

Fig. 11. Schematic real-space energy band diagram of (a) δ-FET, (b) MESFET and (c) HEMT. The δ-FET has the lowest electric field between the 2DEG and the gate, resulting in a high breakdown voltage.

compared to the layer thickness, should exhibit a nearly constant gate–channel capacitance C_{gs} as a function of the gate bias voltage V_{gs}, due to the relatively constant distance between the gate and the depletion boundary that remains within the narrow buried layer. In the δ-doped FET, which is schematically shown in fig. 10, the buried-layer concept is scaled down to its ultimate physical limit normal to the crystal surface, as the narrow buried δ-doping layer has a spatial extent of less than the lattice constant of the GaAs host material. In the early attempts to realize FETs having a δ-doping layer [12], the distance between the gate metal and the electron channel was too large to fully exploit the advantages of this concept. We have recently fabricated δ-FETs with a narrow distance of the 2DEG from the Schottky gate [4,13]. At a distance of 30 nm the depletion region below the gate reaches the δ-doping layer already at zero bias.

In comparison with depletion mode conventional MESFETs and HEMTs, whose conduction band diagrams are also depicted in fig. 11, the advantages of the δ-FET are (i) high electron concentration of the 2 DEG up to 5×10^{12} cm^{-2}, (ii) a large breakdown voltage, and (iii) an intrinsic transconductance exceeding 500 mS/mm owing to the proximity of the electron channel to the gate [4]. Inspection of fig. 11a reveals the constant electric field $\boldsymbol{E}$ between 2DEG and Schottky gate in the δ-FET according to $\boldsymbol{E} = \phi_B/d$, where d is the distance of the 2DEG wavefunction from the gate, because the conduction band edge depends linearly on the spatial coordinate z. In contrast, MESFETs and HEMTs exhibit a quadratic dependence of band-edge variation due to their constant doping concentration below the gate. The electric field between 2DEG and gate is lowest for the δ-FET, resulting in a very high breakdown voltage. The maximum 2D donor concentration of 5×10^{12} cm^{-2} that can be depleted in a δ-FET does not depend on the gate-to-channel distance within a wide range.

The results of a comparison of the calculated intrinsic transconductance of δ-FET and HEMT are shown in fig. 12. For short gate length ($L_G \to 0$) the saturated velocity model applies for the calculation of the maximum intrinsic transconductance

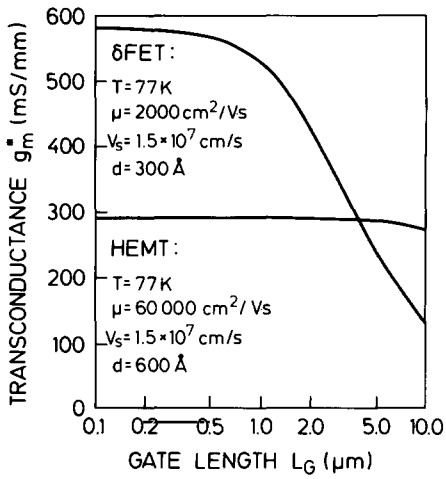

Fig. 12. Calculated transconductances of depletion-mode δ-FET and HEMT using the indicated parameters [4].

g_m^*, according to $g_m^* = \epsilon v_s W_G/d$, where W_G is the gate width, v_s is the electron saturated drift velocity, and ϵ is the permittivity of the semiconductor. This simple equation implies that in addition to the saturated velocity only the distance of the 2DEG from the Schottky gate determines the transconductance of a short-gate FET. Inspection of fig. 12 shows that the HEMT has a higher transconductance for $L_G > 1$ μm, while in short-gate devices ($L_G < 1$ μm) the δ-FET should exceed the performance of the HEMT. In addition, we expect a significant improvement of the high-frequency linearity of the devices due to the linear dependence of C_{gs} upon V_{gs}. Our first preliminary experimental data obtained from a 0.5 μm gate length δ-FET yielded a normalized external transconductance of only 75 mS/mm [13]. This value his now been increases to more than 300 mS/mm by optimizing the device fabrication process of the δ-doped GaAs wafer with the 2DEG 30 nm below the surface [14]. Finally, it is important to note that at the high electric field existing in short-gate FETs the ionized impurity scattering becomes negligible. Therefore, we expect δ-doped layers to have the same saturated drift velocity as homogeneously doped semiconductors or SD heterostructures in short-gate FETs.

4.4. Periodic δ-doping layer structures

Two types of periodic δ-doping layer structures have been conceived: (i) a periodic sequence of δ-doping layers of the same doping type separated by undoped regions which we call δiδi structure, and (ii) a periodic sequence of alternating n- and p-type δ-doping layers equally spaced by undoped regions which we call sawtooth doping superlattice (SDS) due to the space charge induced modulation of the band edges. The thickness of the undoped regions between the δ-doping layers is typically in the range 5 to 20 nm.

The motivation to construct n-type δiδi structures in otherwise intrinsic GaAs comes directly from our experiments on tunnelling through the selfconsistent potential profile described in section 4.2 [9]. For vertical transport in GaAs δiδi structures it is important that the lowest subband level broadens into a 45 meV wide band for 20 nm spaced δ-doping layers with a δ-doping density of 3×10^{12} cm^{-2} [6]. The gap for motion in z-direction is only about 20 meV. The unique shape of the Fermi surface in this GaAs δiδi structure should give rise to novel physical phenomena.

Another motivation for developing δiδi structures in the possibility to realize extremely high 2D doping concentrations in semiconductors, which are several orders of magnitude higher than the solubility limit. For Si-doped GaAs δiδi structures we have achieved equivalent 3D doping concentrations as high as 10^{21} cm^{-3} with a 300 K mobility of 1000 cm^2/V · s. The question to which extent the Si impurities exhibit amphoteric character at these high concentrations needs further clarification. The surface morphology of the Ga δiδi structures remains atomically flat even for δ-doping densities beyond 10^{14} cm^{-2} (15 nm undoped region), and there is no indication for any lattice distortion from high-resolution double-crystal X-ray diffraction measurements. Work is now in progress to construct GaAs/Si superlattices with the constituent Si monolayers lattice matched to GaAs. This superlattice should exhibit exciting new electronic properties.

The motivation for developing GaAs SDS was the requirement for both short carrier lifetimes *and* strong modulation of the energy bands in a

homogeneous semiconductor, in order to achieve stimulated (laser) emission at energies below the bandgap of the host material [3,15]. The doping profile of GaAs SDS, illustrated in fig. 13b, can be described by a periodic train of δ-functions. The periodic variation of the space charge in z-direction leads to a sawtooth-shaped modulation of the conduction and valence band edge, which is schematically shown in fig. 13c for equal 2D donor and acceptor concentrations, i.e. $N_D^{2D} = N_A^{2D} = N^{2D}$. In the narrow V-shaped potential wells size quantization occurs. Radiative recombination in GaAs SDS involves the lowest electron and heavy-hole subband. As a result, the effective superlattice energy gap E_g^{SL} is smaller than the gap of the host material E_g.

In SDS the impurities with discrete charge q are randomly distributed in the respective dopant planes having a mean distance of $(N^{2D})^{-1/2}$. To keep statistical fluctuations of the depth and width of the potential wells low, the mean impurity distance should be less than half the superlattice period, i.e. $\frac{1}{2}z_p < (N^{2D})^{-1/2}$, and the spatial extent of the lowest subband z_0 should be larger than the mean impurity distance, i.e. $z_0 > (N^{2D})^{-1/2}$. At a given doping density N^{2D} the period length z_p determines the quantum mechanical coupling between the V-shaped wells of SDS. Small period lengths imply a strong overlap of electron and hole wavefunctions from adjacent potential wells, which in turn results in short recombination lifetimes in the ns range [3]. This so-called Type A SDS thus exhibits a stable energy gap smaller than the GaAs gap which cannot be tuned by carrier injection. In SDS with long period length, on the other hand, the electron and hole wavefunctions are localized in the respective potential wells, and the radiative recombination probability is low. As a result, in these Type B SDS, long carrier lifetimes and tunable electronic properties similar to those in semiconductors with a "nipi superstructure" can be observed.

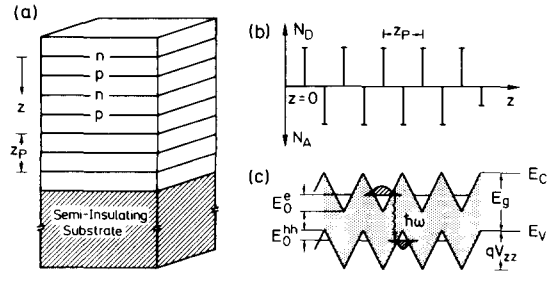

Fig. 13. Schematic illustration of (a) layer sequence, (b) doping profile and (c) modulation of conduction and valence band edges in a GaAs sawtooth doping superlattice.

Photo- and electroluminescence measurements on Type A GaAs SDS of different material design parameters clearly reveal a stable energy gap which is considerably smaller than the gap of the host material and which does not depend on the excitation density [3]. A good agreement of theory and experimental data is observed. The intensity of the superlattice luminescence is high and comparable to bulk-type GaAs, because only transitions between the lowest electron and hole subbands contribute to the observed luminescence and no signal is detected at the GaAs energy gap.

The high intensity and the significant red-shift of the luminescence at 300 K make feasible the application of Type A GaAs SDS in photonic devices. We have fabricated light emitting diodes and injection lasers with the superlattice active region sandwiched by n- and p-type $Al_{0.3}Ga_{0.7}As$ layers for confinement [15]. Edge emitting diodes with different SDS design parameters emit monochromatic light at wavelength of $0.9 \leqslant \lambda \leqslant 1.0$ μm. The threshold current density of broad area lasers emitting at 905 nm was found to be 2.2 kA cm^{-2}.

Acknowledgements

This work was sponsored by the Stiftung Volkswagenwerk and by the Bundesministerium für Forschung und Technologie of the Federal Republic of Germany.

References

[1] C.F.C. Wood, G. Metze, J. Berry and L.F. Eastman, J. Appl. Phys. 51 (1980) 383.

[2] A. Zrenner, H. Reisinger, F. Koch and K. Ploog, in: Proc. 17th Intern. Conf. on Physics of Semiconductors, San Francisco, CA, 1984, Eds. J.D. Chadi and W.A. Harrison (Springer, Berlin, 1985) p. 325.

[3] E.F. Schubert, Y. Horikoshi and K. Ploog, Phys. Rev. B32 1085 (1985).
[4] E.F. Schubert, A. Fischer and K. Ploog, IEEE Trans. Electron Devices ED-33 (1986) 625.
[5] E.F. Schubert and K. Ploog, Japan. J. Appl. Phys. 25 (1986) 966.
[6] F. Koch, A. Zrenner and M. Zachau, Series in Solid State Sciences, Vol. 67 (Springer, Berlin, 1986) p. 175.
[7] Y. Horikoshi, A. Fischer, E.F. Schubert and K. Ploog, Japan, J. Appl. Phys. 25 (1986) 1566.
[8] E.F. Schubert, A. Fischer and K. Ploog, Solid-State Electron. 29 (1986) 173.
[9] M. Zachau, F. Koch, K. Ploog, P. Roentgen and H. Beneking, Solid State Commun. 59 (1986) 591.
[10] R.E. Williams and D.W. Shaw, IEEE Trans. Electron Devices ED-25 (1978) 600.
[11] J.H. Abeles, C.W. Tu, S.A. Schwarz and T.M. Brennan, Appl. Phys. Letters 48 (1986) 1620.
[12] C.E.C. Wood, S. Judaprawira and L.F. Eastman, in: IEDM '79 Tech. Digest (1979) p. 388.
[13] E.F. Schubert and K. Ploog, Japan. J. Appl. Phys. 24 (1985) L608.
[14] E.F. Schubert, J.E. Cunningham, W.T. Tsang and K. Ploog, to be published.
[15] E.F. Schubert, A. Fischer, Y. Horikoshi and K. Ploog, Appl. Phys. Letters 47 (1985) 219.